Ground state of heavy closed shell nuclei: An effective interaction and local density approximation approach

M. Modarres* and N. Rasekhinejad
Physics Department, University of Tehran, 1439955961 Tehran, Iran
(Received 5 September 2005; revised manuscript received 26 September 2005; published 13 December 2005)

We study the ground-state properties of heavy closed-shell nuclei such as ^{48}Ca,^{90} Zr,^{120} Sn, and ^{208}Pb as well as ^{4}He, ^{16}O, and ^{40}Ca. Similar to our recent work, the local density approximation in the harmonic oscillator basis and different channel-dependent effective two-body interactions that are generated through the lowest-order constrained variational calculation for *asymmetric nuclear matter* with the Reid68Day, Reid68, and Δ-Reid68 potentials are used. Unlike nuclear matter, it is shown that Reid68 potential gives ground-state binding energies closer to the experimental data with respect to the Δ-Reid68 potential and there is not much difference between Reid68 and Reid68Day potentials, which have been define up to $J = 5$. The different channel-dependent effective interactions ($J > 2$) and one- and two-body density distribution functions are discussed and they are compared with the results of other approaches such as the Brueckner local density approximation, correlated basis function, variational fermion hypernetted chain, variational cluster Monte Carlo, Brueckner-Hartree-Fock, fermionic molecular dynamics, and coupled cluster. Finally it is concluded that the three-body force (isobar degrees of freedom) is very important for light (heavy) nuclei because in the most of recent many-body calculations, it is observed that the available two-body nuclear forces usually underbind light nuclei and overbind heavy nuclei and nuclear matter.

DOI: 10.1103/PhysRevC.72.064306 PACS number(s): 21.60.Gx, 21.10.Dr, 27.20.+n, 27.40.+z

I. INTRODUCTION

Recently, in the spirit of local density $\mathcal{G}$ matrix, we generated the channel-dependent effective two-body interactions from our lowest-order constrained variational (LOCV) nuclear matter calculation at different densities. We then converted this dependence to a local one by working in the harmonic oscillator basis and the properties of light closed-shell nuclei were calculated. The result was encouraging, with respect to both the available experimental data and different model-dependent theoretical predictions [1].

At present, several nucleon-nucleon potentials are available and most of them reasonably fit the deuteron and N-N scattering phase-shift data. But for many-body theorists during the past five decades, handling such a complicated potential in the finite nuclear systems have been always a difficult task. As a result, usually different approximations and methods have been adopted to overcome this difficulty [2].

The situation is promising for few-body nucleon systems, i.e., $A = 3$–7. The Faddeev, Green function Monte Carlo, and correlated hyperspherical harmonics expansion (CHHE) [3] theories were developed and satisfactory results were reproduced. Conversely, $7 \leqslant A \leqslant 16$ light nuclei are described by the variational or cluster Monte Carlo (VMC and CMC respectively) technique by using the Jastrow variational wave function [4]. The VMC or CMC formalism is very involved and its accuracy is uncertain [1,4]. However, there is little hope for these methods to be applicable to heavy nuclei such as ^{208}Pb, at the very least because of the enormous computation time.

There is no finite size problem for infinite nucleonic matter, but one needs a reliable many-body technique and a true nucleon-nucleon potential to obtain reliable results. It was reported in several of our works (using the LOCV method) [5] that the many-body calculations on nuclear matter with phenomenological potentials such as Reid68 [6] give substantially too much binding and large saturation density. Over the past three decades, the situation has been the same for other techniques and potentials [7,8]. But the inclusion of three-body force and Δ isobar degrees of freedom (Δ-Reid68) [1,6] have improved the behavior of the Coester line to the right direction [2].

Since then, a few number of sophisticated interactions such as the UV_{14} [8], the AV_{14} [9] and the new Argonne AV_{18} [10] as well as Reid93 [11] potentials have been generated and used. These potentials fit the N-N scattering data very well [11]. But they still overbind nuclear matter at large saturation densities.

A very good agreement has been found between the LOCV technique [12,13] and the results of more sophisticated methods such as variational fermion hypernetted chain (FHNC) calculations [12,13] at both zero and finite temperatures. But in most of these works the many-body calculations with the new potentials, such as the old Reid68 potential, overbind nuclear matter with a larger density than that predicted empirically.

The LOCV method was also applied to finite nuclei [14] for which there was some difficulty in defining the long-range behavior of the correlation functions and the resulting binding energy calculations for the light nuclei were not satisfactory [1,14,15].

With respect to the above arguments in this article we intend to extend our recent work [1] to heavier nuclei, such as ^{48}Ca,^{90} Zr,^{120} Sn, and ^{208}Pb, in the harmonic oscillator basis by using the local density approximation and the channel-dependent effective two-body interactions that are generated through our LOCV *asymmetric nuclear matter* code with the Reid68, Δ-Reid68, and Reid68Day [5,6] potentials. For the

*Electronic address: modarres@khayam.ut.ac.ir

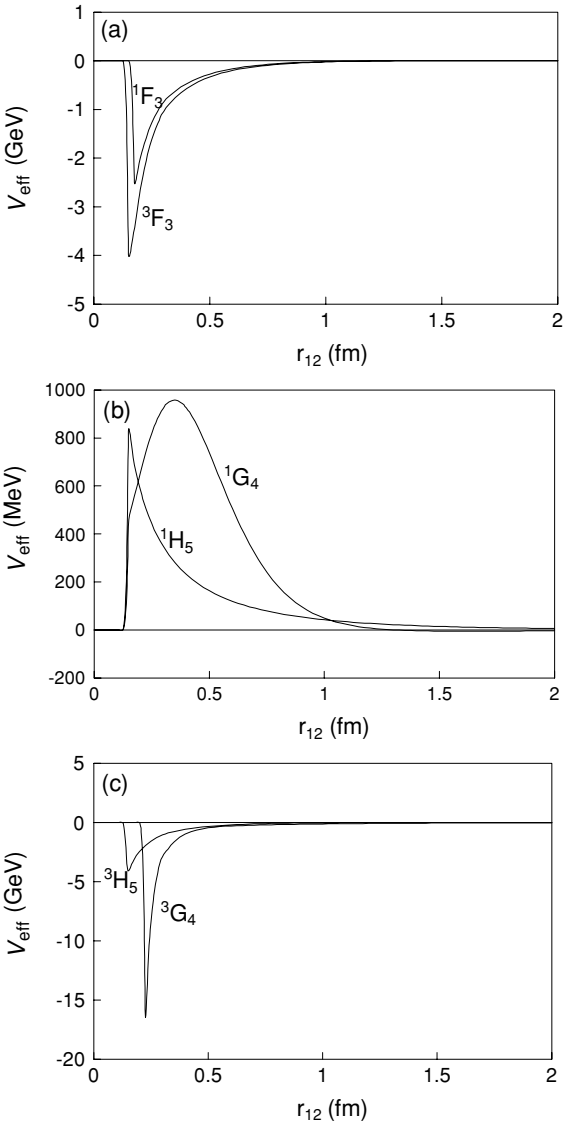

FIG. 1. The channel-dependent effective two-body interactions ($J > 2$) with Reid68Day potential at nuclear matter saturation density, $\rho = 0.17\,\mathrm{fm}^{-3}$, versus r_{12} (fm) for uncoupled channels.

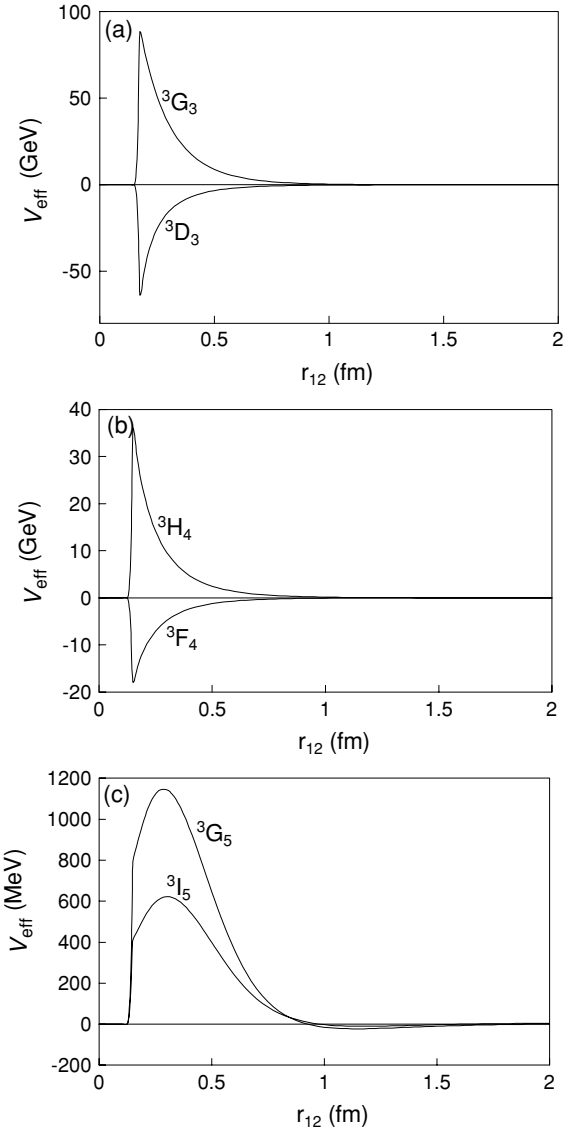

FIG. 2. As in the legend to Fig. 1 but for the coupled channels.

latter case, we also reexamine the properties of ^{4}He, ^{16}O, and ^{40}Ca [1]. Then we can compare present results with those of Brueckner local density approximation (LDA) [16], coupled cluster (CCM) [17], correlated basis function (CBF-FHNC) [18–24], VMC or CMC [4], Brueckner-Hartree-Fock (BHF) [25,26] and fermionic molecular dynamics (FMD) [27] calculations that have been presented recently and most of them need enormous computational time on super- or main-frame computers. A comparison is also made with the present available data [28].

We prefer to focus on Reid-type potentials that are state-dependent and do not use the recent phenomenological potentials such as AV_{18} [10], because in our previous calculations we have found that these potentials do not predict the empirical saturation properties of nuclear matter [13] correctly and they are not much different from the old Reid68 potential. This point has been also reported by other groups [12,18–27]. However, our recent works on nuclear matter [29] show that the new Reid potential, Reid93 [11,30], overbinds nuclear matter at much higher saturation densities than Reid68 and the results are very similar to those of Reid68Day. However, the Reid68 and Reid93 potentials give the same saturation properties for nuclear matter up to $J = 2$ channels [29]. But the present available calculations on finite nuclei show that the nucleus properties, unlike nuclear matter, are not very sensitive to the choice of potentials [1,18–27] (especially for the light nuclei). One reason could be the low density properties of nuclei with respect to the nuclear matter, i.e., the long range parts of different nucleon-nucleon potentials are roughly the same and there are always a balance between the central and tensor components of the N-N forces.

The article is as follows: Because for heavy nuclei we have different numbers of protons (Z) and neutrons (N), a short description of the lowest order constrained variational method for *asymmetric nuclear matter* and the calculation of

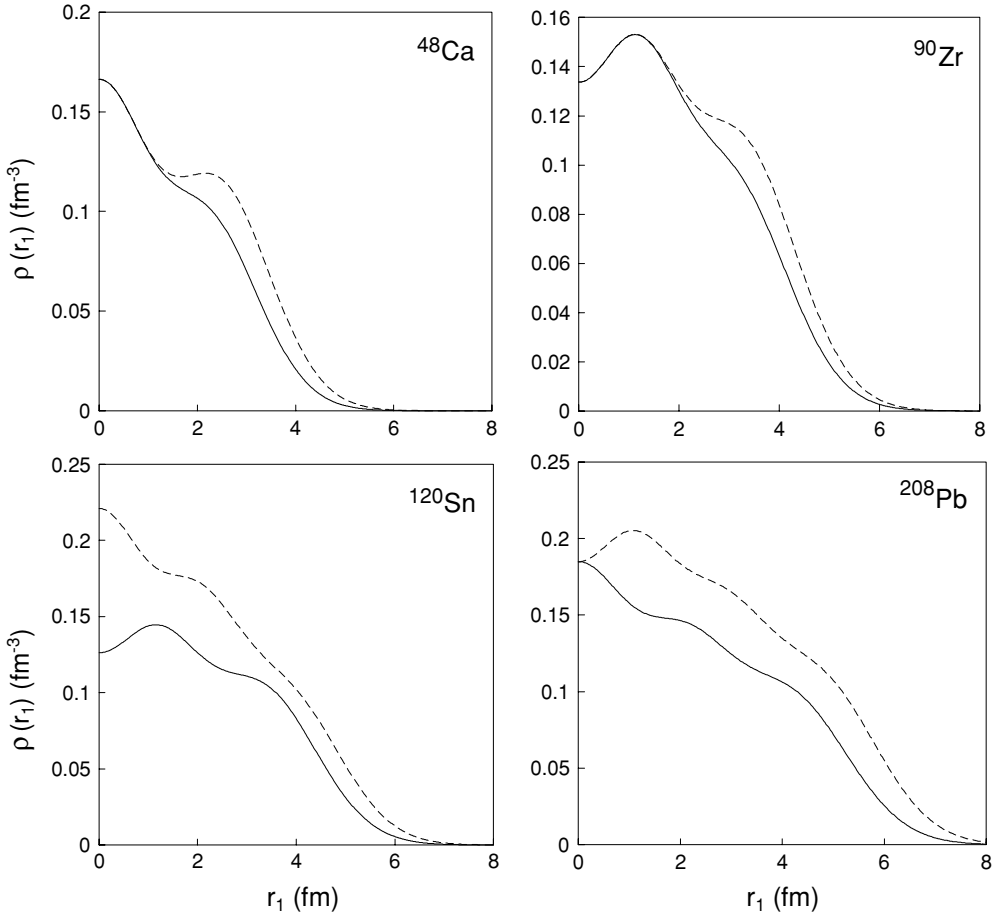

FIG. 3. The one-body density distributions for different heavy closed shell nuclei at their saturation energies with Reid68 potential. Full (dotted) curves are the corresponding proton (neutron) density.

channel-dependent effective two-body interactions are given in the appendix. Section II is devoted to the evaluation of matrix elements and the binding energies of different closed-shell nuclei by using the local density approximation. Finally, in Sec. III we present the results and discussions.

II. THE BINDING ENERGY OF HEAVY CLOSED-SHELL $N \neq Z$ NUCLEUS

Because the finite nuclei are localized, we no longer have the translation invariance that characterized the *asymmetric nuclear matter* calculations. Regarding our recent calculation on light closed-shell nuclei, we simply assume that the single-particle states, ϕ_i, may be approximated by the harmonic oscillator wave functions, leaving the oscillator energy $\hbar\omega$ as a single variational parameter to fix the root-mean-square (rms) radius of the specific nucleus. Here, we assume the following configurations for different closed-shell nuclei:

$$
\begin{aligned}
&^4\mathrm{He}: (0s)^4\\
&^{16}\mathrm{O}: (^4\mathrm{He}) + (0p)^{12}\\
&^{40}\mathrm{Ca}: (^{16}\mathrm{O}) + (0d)^{20}(1s)^4\\
&^{48}\mathrm{Ca}: (^{40}\mathrm{Ca}) + (0f_{7/2})_n^8\\
&^{90}\mathrm{Zr}: (^{40}\mathrm{Ca}) + (0f)^{28}(1p)^{12}(0g_{9/2})_n^{10}\\
&^{120}\mathrm{Sn}: (^{40}\mathrm{Ca}) + (0f)^{28}(1p)^{12}(0g_{9/2})^{20}\\
&\qquad \times (0g_{7/2})_n^8(1d)_n^{10}(2s)_n^2\\
&^{208}\mathrm{Pb}: (^{40}\mathrm{Ca}) + (0f)^{28}(1p)^{12}(0g)^{36}(1d)^{20}(2s)^4\\
&\qquad \times (0h_{11/2})^{24}(0h_{9/2})_n^{10}(1f)_n^{14}(2p)_n^6(0i_{13/2})_n^{14}. \qquad (1)
\end{aligned}
$$

The origin of our coordinate is fixed at the center of mass of the nucleus, $\sum_{i=1}^{A} \mathbf{r_i} = 0$. Then we should consider only the intrinsic Hamiltonian,

$$\mathcal{H}_0 = \mathcal{H} - \frac{\mathcal{P}^2}{2\mathcal{M}}, \qquad (2)$$

where $\mathcal{P} = \sum_i \mathbf{p_i}$ and $\mathcal{M} = Am$ are the nucleus total momentum and mass, respectively.

Now, in the harmonic oscillator basis we should calculate the expectation value of $\mathcal{H}_0$,

$$
\begin{aligned}
E^{\mathrm{B.E.}}_{\mathrm{Total}} = \langle \mathcal{H}_0 \rangle &= \sum_i \langle i, \hbar\omega | \frac{p^2}{2m} | i, \hbar\omega \rangle\\
&+ \frac{1}{2} \sum_{ij} \langle ij, \hbar\omega | \mathcal{V}(12) | ij, \hbar\omega \rangle_a - T^A_{\mathrm{C.M.}}, \qquad (3)
\end{aligned}
$$

where $T^A_{\mathrm{C.M.}} = \frac{3}{4}\hbar\omega$ and $|i, \hbar\omega\rangle$ stands for $|n_i, l_i, s_i, \tau_i, m_{\tau_i}; \hbar\omega\rangle$, the harmonic oscillator wave functions, angular, spin,

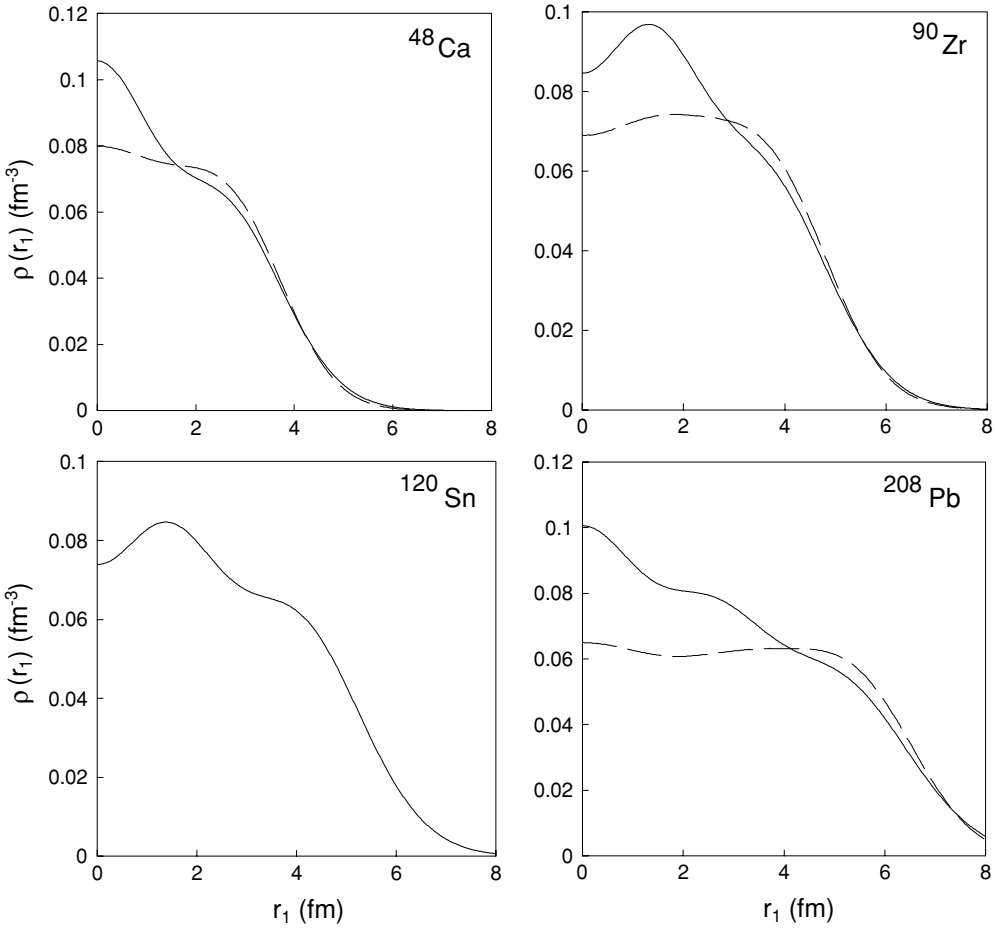

FIG. 4. The one-body density distributions (proton) for different heavy closed-shell nuclei at experimental rms charge radius. The dash curves are the experimental charge distributions [28].

isospin, and isospin projection parts of single-particle states, respectively. As pointed out before, $\hbar\omega$ or $\gamma = \sqrt{m\omega/\hbar}$ is the harmonic oscillator parameter and is fixed variationally. The matrix element of one-body kinetic energy per nucleon (first term) has the familiar form:

$$T_1 = \frac{1}{2A}\sum_{i=1}^{A}\left(2n_i + l_i + \frac{3}{2}\right)\hbar\omega, \tag{4}$$

whereas the second term can be written as the sum of two-body kinetic and potential energies per nucleon (see the appendix and Refs. [1,29]):

$$\begin{aligned} E_2 = T_2 + V_2 &= \frac{1}{2A}\sum_{ij}\langle ij,\hbar\omega|\mathcal{V}(12)|ij,\hbar\omega\rangle_a \\ &= \frac{1}{2A}\sum_{ij}\langle ij,\hbar\omega| \\ &\quad -\frac{\hbar^2}{2m}\big[F(12),\big[\nabla_{12}^2, F(12)\big]\big]|ij,\hbar\omega\rangle_a \\ &\quad +\frac{1}{2A}\sum_{ij}\langle ij,\hbar\omega|F(12)V(12)F(12) \\ &\quad \times |ij,\hbar\omega\rangle_a. \end{aligned} \tag{5}$$

Then by using Eqs. (A5)–(A7) we can write our effective two-body interactions as follows:

$$\mathcal{V}_{\rm eff}^{k,l}(r_{12}, R_{12};\mathcal{R}) = \sum_{\alpha}\mathcal{V}_{\alpha}^{k,l}\left(\sqrt{2}r, \rho\left(\frac{R}{\sqrt{2}};\mathcal{R}\right)\right)|\alpha\rangle\langle\alpha| \tag{6}$$

with

$$\mathbf{r} = \frac{1}{\sqrt{2}}(\mathbf{r_1} - \mathbf{r_2}) = \frac{1}{\sqrt{2}}\mathbf{r_{12}}, \mathbf{R} = \frac{1}{\sqrt{2}}(\mathbf{r_1} + \mathbf{r_2}) = \sqrt{2}\mathbf{R_{12}}. \tag{7}$$

Next for the two-body energy, we have assumed $\alpha = lJSTM_T$, $[j] = 2j+1$, and so on, and first and second curly brackets are the 6-j and 9-j symbols, respectively, in

$$\begin{aligned} E_2 = \frac{1}{2A}\sum_{1,2,k,i,\alpha'} &[j_1][j_2][j][\lambda]^2[S][J]\left|\left\langle m_{\tau_1}m_{\tau_2}\middle|T, M_T\right\rangle\right|^2 \\ &\times (1-(-1)^{l+S+T})\begin{Bmatrix} L & l & \lambda \\ S & j & J\end{Bmatrix}^2\begin{Bmatrix} l_1 & \frac{1}{2} & j_1 \\ l_2 & \frac{1}{2} & j_2 \\ \lambda & S & j\end{Bmatrix}^2 \\ &\times \langle n_1l_1, n_2l_2, \lambda|nl, NL, \lambda\rangle^2\langle nlJSTM_T, NL| \\ &\times \mathcal{V}_{\alpha}^{k,i}\left(\sqrt{2}r, \rho\left(\frac{R}{\sqrt{2}};\mathcal{R}\right)\right)\{|\alpha'\rangle\langle\alpha'|\}\,|\,nlJSTM_T, NL\rangle, \end{aligned} \tag{8}$$

TABLE I. The variational binding energies (mega-electron-volts) per nucleon of closed shell nuclei (^{4}He, ^{16}O, and ^{40}Ca) by using the channel dependent effective two-body interactions base on the *asymmetric nuclear matter* LOCV calculation with Reid68Day, Reid68, and Δ-Reid68 interactions. See the text for explanation about different columns.

Nucleus	Potential	γ	T	T_2	V_2	BE	V_c	BE$_c$	$r_{\rm rms}$	BE$^{\rm exp.}$	$r_{\rm rms}^{\rm exp.(ch)}$
^{4}He	Reid68Day	0.69	10.97	8.78	−23.15	−3.40	0.20	−3.21	1.77	−7.08	1.63
	Reid68	0.69	11.10	9.85	−25.34	−4.38	0.20	−4.19	1.77		
	Δ-Reid68	0.64	9.55	13.99	−25.87	−2.32	0.18	−2.14	1.91		
^{16}O	Reid68Day	0.63	17.79	13.99	−37.21	−5.43	0.94	−4.49	2.38	−7.98	2.65
	Reid68	0.61	16.64	14.07	−36.89	−6.18	0.90	−5.28	2.46		
	Δ-Reid68	0.57	14.52	20.07	−37.81	−3.21	0.83	−2.38	2.63		
^{40}Ca	Reid68Day	0.59	21.48	18.17	−48.70	−9.05	2.08	−6.97	2.94	−8.55	3.39
	Reid68	0.57	19.96	17.95	−47.11	−9.20	1.91	−7.30	3.04		
	Δ-Reid68	0.54	17.91	26.49	−49.85	−5.45	1.91	−3.69	3.21		

where we consider the local density approximation [1,14–16] and we replace

$$\tfrac{1}{2}[\rho(|\mathbf{r_1}|;\mathcal{R}_1)+\rho(|\mathbf{r_2}|;\mathcal{R}_2)] \tag{9}$$

with the following (note that the local density approximation is especially valid when we have short range forces):

$$\rho\left(\left|\frac{\mathbf{R}}{\sqrt{\mathbf{2}}}\right|;\mathcal{R}\right)=\rho\left(\frac{|\mathbf{r_1}+\mathbf{r_2}|}{2};\mathcal{R}\right),\mathcal{R}(|\mathbf{R}|)=\frac{\rho_p(|\mathbf{R}|)}{\rho_n(|\mathbf{R}|)}. \tag{10}$$

The $\langle n_1 l_1, n_2 l_2, \lambda \mid nl, NL, \lambda\rangle$ are the familiar Brody-Moshinsky brackets [31]. The uncorrelated one-body density is defined as following in terms of the harmonic oscillator wave functions for each nucleus,

$$\rho(|\mathbf{r_j}|;\mathcal{R}_\mathbf{j})=\rho_p(|\mathbf{r_j}|)+\rho_n(|\mathbf{r_j}|),\quad \mathcal{R}_\mathbf{j}(|\mathbf{r_j}|)=\frac{\rho_p(|\mathbf{r_j}|)}{\rho_n(|\mathbf{r_j}|)}, \tag{11}$$

where

$$\rho_p(|\mathbf{r_j}|)=\sum_i^Z|\langle\mathbf{r_j}|i,\hbar\omega\rangle|^2,\quad \rho_n(|\mathbf{r_j}|)=\sum_i^N|\langle\mathbf{r_j}|i,\hbar\omega\rangle|^2. \tag{12}$$

We can also define the two-body correlated distribution function [32] for the above nuclei as follows [1]:

$$\begin{aligned}\rho_2^p(\mathbf{r_1},\mathbf{r_2};\mathcal{R})&=\rho_2^p(\mathbf{r_{12}},\mathbf{R_{12}};\mathcal{R}(|\mathbf{R}_{12}|))\\&=\left[\sum_i^Z|\langle\mathbf{r_1}|i,\hbar\omega\rangle|^2\sum_j^Z|\langle\mathbf{r_2}|j,\hbar\omega\rangle|^2\right.\\&\quad\left.-\left|\sum_i^Z\langle\mathbf{r_1}|i,\hbar\omega\rangle\langle i,\hbar\omega,|\mathbf{r_2}\rangle\right|^2\right]\\&\quad\times\mathcal{F}^2(|\ \mathbf{r_{12}}\ |,\rho(|\mathbf{R_{12}}|;\mathcal{R}(|\mathbf{R}_{12}|)))\end{aligned} \tag{13}$$

with correlated one-body density

$$\bar{\rho}_p(\mathbf{r_1})=\frac{1}{Z-1}\int d\mathbf{r_2}\rho_2^p(\mathbf{r_1},\mathbf{r_2};\mathcal{R}) \tag{14}$$

and correlated relative two-body density

$$\bar{\rho_2^p}(\mathbf{r_{12}})=\frac{1}{Z}\int d\mathbf{R_{12}}\rho_2^p(\mathbf{r_1},\mathbf{r_2};\mathcal{R}) \tag{15}$$

distributions. Obviously we should have the normalization integral,

$$\frac{1}{Z(Z-1)}\int\rho_2^p(\mathbf{r_1},\mathbf{r_2};\mathcal{R})d\mathbf{r_1}d\mathbf{r_2}=1. \tag{16}$$

Note that the same equations, i.e., Eqs. (13)–(16), are valid for the neutrons as well. Now, we can easily calculate the heavy nucleus binding energy per nucleon as follows:

$$\mathcal{E}_A^{\rm B.E.}=\frac{1}{A}E_{\rm Total}^{\rm B.E.}=[T_1+T_2+V_2-T_{\rm C.M.}]. \tag{17}$$

III. RESULTS AND DISCUSSION

The LOCV effective two-body interactions for the new channels, $3\leqslant J\leqslant 5$, by using Reid68Day potential are given in Figs. 1 (uncoupled) and 2 (coupled) [see Eqs. (A5) and (A6)] at nuclear matter saturation density $\rho=0.17\,\mathrm{fm}^{-3}$. The $J\leqslant 2$ channels are not much different from the LOCV calculations with Reid68 potential and they have been discussed in details in Ref. [1]. The two-body kinetic parts of effective interactions for the new channels are very small with respect to their potential parts. Conversely, their interaction ranges are much shorter than $J\leqslant 2$ channels and they are either attractive or repulsive. As pointed out in Ref. [29] and as we show later, only the $J=3$ channels have noticeable repulsive contributions to the binding energies. The repulsive and attractive behaviors of effective interactions are mainly because the definition form of the Reid68Day potential, because their two-body kinetic parts are roughly zero.

Table I shows the variational binding energies of light closed-shell nuclei, ^{4}He, ^{16}O, and ^{40}Ca, with and without Coulmb energies by using Reid68Day, Reid68, and Δ-Reid68 potentials. For each nucleus the oscillator parameter, the one-body ($T=T_1-T_{\rm C.M.}$) and two-body kinetic energies, the two-body potential energy, the calculated rms radius, the experimental binding energy, and the rms charge radius are also given for comparison. For the $J>5$ we have used the averaged effective interactions defined in Ref. [1]. The result of our recent calculation with Reid68 and Δ-Reid68 potentials are also given in this table for comparison. There are few differences between the results of calculations with the

TABLE II. The same as Table I but for heavy closed-shell nuclei, i.e., ^{48}Ca,^{90} Zr,^{120} Sn, and ^{208}Pb.

Nucleus	Potential	γ	T	T_2	V_2	BE	V_c	BE$_c$	$r^n_{\rm rms}$	$r^p_{\rm rms}$	BE$^{\rm exp.}$	$r^{\rm exp.(ch)}_{\rm rms}$
^{48}Ca	Reid68Day	0.60	24.14	19.39	−52.34	−8.81	1.77	−7.04	3.09	2.89	−8.67	3.53
	Reid68	0.57	21.68	18.64	−49.30	−8.97	1.67	−7.30	3.25	3.04		
	Δ-Reid68	0.54	19.46	27.60	−52.09	−5.04	1.47	−3.57	3.43	3.21		
^{90}Zr	Reid68Day	0.57	26.51	23.02	−61.75	−12.22	3.32	−8.90	3.55	3.40	−8.71	4.27
	Reid68	0.53	22.88	20.84	−55.35	−11.64	3.06	−8.58	3.82	3.65		
	Δ-Reid68	0.51	21.18	32.05	−60.49	−7.25	2.73	−4.53	3.97	3.80		
^{120}Sn	Reid68Day	0.56	28.09	24.73	−65.91	−13.09	3.67	−9.42	3.79	3.62	−8.50	4.65
	Reid68	0.52	24.22	22.42	−59.07	−12.43	3.39	−9.04	4.08	3.89		
	Δ-Reid68	0.49	21.51	32.95	−62.18	−7.72	3.03	−4.69	4.32	4.13		
^{208}Pb	Reid68Day	0.52	28.68	25.05	−68.33	−14.60	4.86	−9.74	4.51	4.21	−7.87	5.52
	Reid68	0.49	25.95	24.10	−63.84	−13.78	4.57	−9.22	4.79	4.47		
	Δ-Reid68	0.46	22.87	35.30	−66.85	−8.68	4.10	−4.58	5.10	4.76		

Reid68Day and Reid68 potentials. The Reid68Day potential gives roughly 5% less (50% more, which is mainly because of the two-body kinetic energy) binding than that of Reid68 (Δ-Reid68). We obtain a reasonable rms radius with respect to the experimental data for the whole range of light closed-shell nuclei. The binding energies are close to their corresponding experimental values as the nuclear mass increases, especially in case of the Reid68 potential. The one- and two-body kinetic energies have roughly the same size and the two-body potential energies are also approximately twice as large as each of them (in addition to the Δ-Reid68 potential).

The variational binding energies of heavy closed-shell nuclei, ^{48}Ca,^{90} Zr,^{120}Sn, and ^{208}Pb, with the Reid68Day, Reid68, and Δ-Reid68 potentials are given in Table II. We obtain much better agreement between the calculated and experimental binding energy and rms radius with respect to that of light closed-shell nuclei, i.e., we overbind ^{120}Sn and ^{208}Pb and under bind light nuclei with the Reid68Day and Reid68 potentials. In the latter case the three-body force should be included to get a good agreement with the experimental result. Other groups obtain the same result. We obtain a result for medium nuclei, i.e., ^{40}Ca,^{48}Ca, and ^{90}Zr, that is very close to the experimental results. So we can conclude that for medium-heavy nuclei the three-body force and isobar degrees of freedom cancel each other.

Table III shows the channel breakdown of two-body kinetic, potential, and Coulmb energies for ^{90}Zr with Reid68 and Reid68Day potentials. For $J > 3$ in Reid68 potential and for $J > 5$ in Reid68Day potential we have used the averaged effective two-body interactions discussed in Ref. [1]. Only in case of Reid68Day the potential energy have reasonable attractive contribution for $3 \leqslant J \leqslant 5$. Which is mainly comes from $J = 3$ channels as have been pointed out in Ref. [29] and it is demonstrated in this table.

In Table IV we have compared our calculated binding energy and rms radius for light and heavy closed-shell nuclei with different approaches, namely local density approximation (LDA) of Negele [16], coupled cluster (CCM-FBHF3) of Kümmel *et al.* [17], cluster or variational Monte Carlo (CMC,VMC) of Pieper *et al.* [4], CBF-FHNC of Fabrocini *et al.* [18,19] and Arias de Saavedra *et al.* [22,23] (with both harmonic oscillator and Woods-Saxon basis), Brueckner-Hartee-Fock (BHF) of Coraggio *et al.* [25,26] with N^{3}LO and AV_{18} interactions and Fermionic molecular dynamics (FMD) of Roth *et al.* [27]. The LDA and CCM calculation are with Gammel-Thaler and Reid68 potential [6,16], whereas the other methods have used UV_{14} or AV_{18} plus three-body interaction (TBI). We have not included TBI in our calculation. Its contribution is a binding of ∼1 MeV. So by comparison we can conclude that we obtain a reasonable result, especially

TABLE III. The channel breakdown two-body kinetic, potential, and Coulmb energies for ^{90}Zr with Reid68Day and Reid68 potentials.

J	Reid68Day			Reid68		
	T_2	V_2	V_c	T_2	V_2	V_c
0	7.7145	−25.9505	0.6932	6.9472	−23.8099	0.6426
1	15.1931	−19.6060	0.5341	13.6497	−20.0020	0.4942
2	0.1091	−13.4839	1.4073	0.1772	−10.5649	1.2994
3	0.0021	−2.3934	0.2062	0.0508	−0.6542	0.1889
4–9	0.0006	−0.3149	0.4825	0.0106	−0.3210	0.4379
0–9	23.02	−61.75	3.32	20.84	−55.35	3.06

TABLE IV. The comparison of our calculated ground-state binding energies per nucleon (mega-electron-volts) and rms radius (fm) of ^{4}He, ^{16}O, ^{40}Ca, ^{48}Ca, ^{90}Zr, and ^{208}Pb nuclei for three N-N potentials, Δ-Reid68 (LOCV-ΔR68), Reid68Day (LOCV-R68D), and Reid68 (LOCV-R68) with different models and experimental data (Exp.).

Model	^{4}He		^{16}O		^{40}Ca		^{48}Ca		^{90}Zr		^{208}Pb	
	BE	$\langle r\rangle$	BE	$\langle r\rangle$	BE	$\langle r\rangle$	BE	$\langle r\rangle$	BE	$\langle r\rangle$	BE	$\langle r\rangle$
LDA [16]	—	—	−6.75	2.71	−7.49	3.41	−7.48	3.45	−7.85	4.18	−7.53	5.37
FBHF3 [17]	−5.75	1.63	−5.36	2.57	−5.64	3.17	—	—	—	—	—	—
CMC [4]	−7.6	—	−7.7	—	—	—	—	—	—	—	—	—
FHNC [22]	—	—	−9.26	—	−10.62	—	−9.66	—	—	—	−9.62	—
FHNC [18]	—	—	−5.15	2.32	−7.87	2.87	—	—	—	—	—	—
FHNC [19]	—	—	−5.11	2.93	−6.50	3.66	—	—	—	—	—	—
FHNC-HO [23]	—	—	−7.07	2.43	−9.00	3.08	−7.57	3.00	−10.07	3.57	−10.24	4.67
FHNC-WS [23]	—	—	−6.29	2.69	−8.12	3.29	−6.79	3.35	−7.30	4.09	−8.03	5.52
BHF [25]	—	—	−7.52	2.65	−9.19	3.44	—	—	—	—	—	—
BHF [26]	−6.85	1.69	−8.26	2.59	−9.53	3.22	—	—	—	—	—	—
FMD [27]	−6.99	1.51	−7.40	2.25	−8.19	2.89	−7.87	2.93	—	—	—	—
LOCV-ΔR68	−2.14	1.91	−2.38	2.63	−3.69	3.21	−3.57	3.21	−4.53	3.80	−4.58	4.76
LOCV-R68D	−3.21	1.77	−4.49	2.38	−6.97	2.94	−7.04	2.89	−8.90	3.40	−9.74	4.21
LOCV-R68	−4.19	1.77	−5.28	2.46	−7.30	3.04	−7.30	3.04	−8.58	3.65	−9.22	4.47
Exp.	−7.08	1.63	−7.98	2.65	−8.55	3.39	−8.67	3.53	−8.71	4.27	−7.87	5.52

for $A \geqslant 40$ (medium and heavy nuclei) with respect to both experimental data and others theoretical calculations. It is worth saying that for each harmonic oscillator parameter the calculation for ^{208}Pb takes about 6 hr on a Pentium IV 2400-MHz personal computer. So, as we pointed out in Ref. [1], this can be, for example, compared with the CMC calculation for ^{16}O, estimated to take at least 10 hr of computer time (Cray-2 supercomputer).

By using Eqs. (13)–(16), in the Fig. 3, the one-body densities for proton (neutron) are presented for the heavy closed-shell nuclei, i.e., ^{48}Ca, ^{90}Zr, ^{120}Sn, and ^{208}Pb by full (dotted) curves. They have been calculated at their saturation energies with Reid68 potential. At these points the rms radius of neutron and proton are given in Table II for comparison. Obviously, the neutron rms is much larger than that of proton and the differences are increased as we go to heavier nuclei. Figure 4 shows the one-body proton distributions of above heavy closed-shell nuclei at their experimental rms charge radius by using only pure harmonic oscillator wave functions. The dash curves are the experimental charge distributions for ^{48}Ca, ^{90}Zr, and ^{208}Pb [28]. In general we get smaller charge rms radius with respect to the experimental predictions. The calculated proton distributions for ^{48}Ca, ^{90}Zr, and ^{208}Pb are in good agreement with the data [28] beyond 3 fm. So, as usual, we can not get results close to the experimental data even by including short-range correlations. In Ref. [1] we showed that the effect of correlation is small and decreases as the nuclear mass is increased. We found that for heavy nuclei this correlation is much smaller. The comparison of one-body correlated proton distributions, by using the $^{3}S_1$ correlation function (that of Reid68) that has the largest correlation range with respect to other channels (dotted curves), and that of uncorrelated (full curves) ones and their differences for heavy closed shell nuclei are plotted in Figs. 5(a) and (b), respectively. It is seen that even with $^{3}S_1$ correlation function,

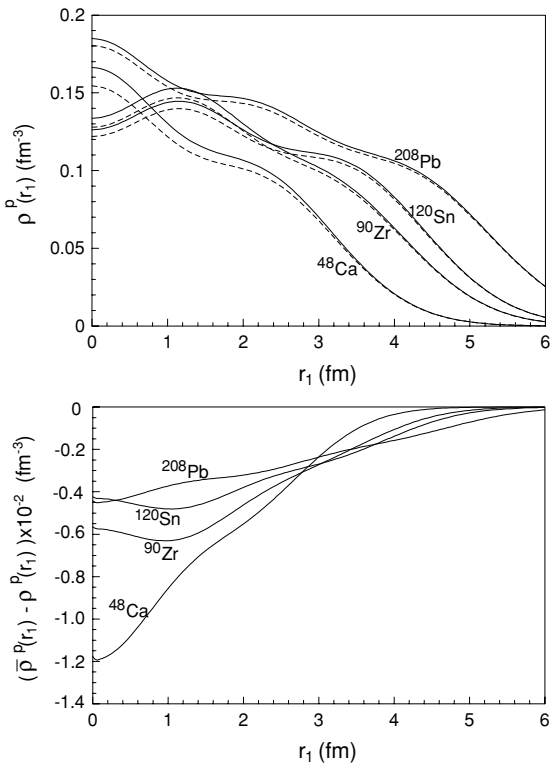

FIG. 5. The proton one-body density distributions without (with) two-body correlation functions, full (dotted) curves. (b) The difference between the correlated and pure harmonic oscillator proton one-body density distributions at our calculated saturation binding energies.

the short-range correlations have very small effect at short distances and the effect becomes negligible as we go to the larger distances and heavier nuclei (note that the electromagnetic

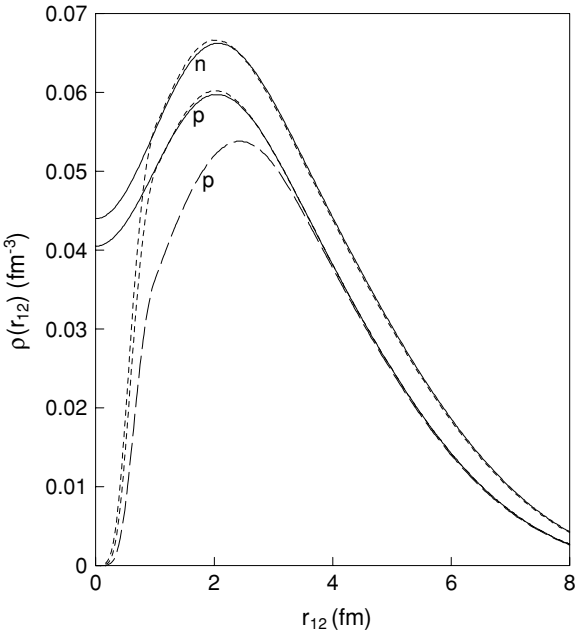

FIG. 6. The relative two-body density distributions without (with) two-body correlation functions, full (dotted) curves. The dash curve is the one with $^3S_1$ correlation function in all of the channels.

form factor of nucleons have not been folded in our calculated one-body densities).

Finally in Fig. 6 the correlated relative two-body neutron and proton distributions (dotted curves) are given for ^{90}Zr nucleus at the saturation energy by using Reid68 potential (the rms radius for each distribution is given in Table II). The full curves are the uncorrelated ones. The dash curve has been calculated by using the $^3S_1$ correlation function in all of the channels. As we pointed out before, the $^3S_1$ correlation function has the longest range with respect to other channel correlation functions. So, the correlation affects only the distances less than 3 fm and the largest shift we can have with respect to the uncorrelated situation is the dash curve. We can conclude that to describe the short-range part of one-body distribution one should consider other effects such as the inclusion of finite size effect and quark degrees of freedom for the nucleon to get a reasonable agreement with the experimental data. It is worth to point out here that the normalization integral, Eq. (16), is satisfied in our calculation roughly with values of 0.9992, 0.9958, 0.9910, and 0.9909 for ^{48}Ca, ^{90} Zr, ^{120}Sn, and ^{208}Pb (at their saturation energies) for Reid68 potential, respectively. Which is less than 1%.

In conclusion, we have calculated the binding energy of light, medium, and heavy closed-shell nuclei by considering the local density approximation and the effective interaction that is generated through the reliable method such as LOCV formalism with Reid68, Reid68Day, and Δ-Reid68 potentials. One can argue that we do not know how accurate the above approximations are; we imposed the truncation on the configuration space. However, it is encouraging that our results are in agreement with those of other methods in which more complicated formalism and computer simulations have been used. Our binding energy results with Reid68 and Reid68Day potentials become closer to those of the experimental data as we go to the heavier closed-shell nuclei. As in our previous work [1] we found that the saturation curves are sensitive to the γ, the harmonic oscillator parameter. This indicates that we should take wider range of harmonic oscillator wave functions as our single-particle states [including all of principle quantum numbers pairs (n_1, n_2)].

We can improve our result by taking into the account the three-body forces and using the present *asymmetric nuclear matter* code with the new charge-dependent potentials to look into charge-symmetric breaking in nuclei or including the averaged three-body cluster effective interaction into present channel-dependent effective two-body interactions to investigate the three-body correlations in nuclei.

Finally, as already pointed out, we make the general remark that most of present available many-body calculations on light, medium, and heavy nuclei and nuclear matter show that the three-body forces (isobar degrees of freedom, i.e., the effect of mean field on the intermediate states etc.) are much important for light nuclei (heavy nuclei and nuclear matter), because in these works the two-body force that has been fitted to reproduce the phase-shift data will underbind light nuclei and overbind heavy nuclei and nuclear matter.

ACKNOWLEDGMENTS

M. M. thanks University of Tehran for supporting him under the grants provided by its Research Council and N. R. thanks Dr. Moshfegh for many useful discussions.

APPENDIX: THE LOCV FORMALISM AND ISOSPIN DEPENDENCE OF EFFECTIVE INTERACTIONS

A general discussion about the LOCV formalism can found in Sec. II of our recent works [1,29]. The main differences for *asymmetric nuclear matter* calculation come from the boundary conditions and the definition of effective interactions which are as follows:

In general, the N-Δ correlation function $f_\alpha^{(4)}$ is required to heal to zero, whereas the rest of the channel correlation functions $f_\alpha^{(1)}$, $f_\alpha^{(2)}$, and $f_\alpha^{(3)}$ heal to the iso-spin dependence modified Pauli function $f_P^{M_T}(r)$ $(i = p, n)$,

$$f_P^{M_T}(r) = \left\{1 - \frac{1}{2}\left[l\left(k_F^i r\right)\right]^2\right\}^{-\frac{1}{2}} \quad n\text{-}n \quad \text{and} \quad p\text{-}p \quad \text{channels } (M_T = -1, 1)$$
$$= 1\, n\text{-}p \quad \text{channels } (M_T = 0) \tag{A1}$$

with

$$l(x) = \frac{3}{2x}\mathcal{J}_1(x), \tag{A2}$$

where $\mathcal{J}_J(x)$ are the familiar spherical Bessel functions, k_F^i are the Fermi momenta that are fixed by the *asymmetric nuclear matter* density $\rho(\mathcal{R})$, $k_F^i = (3\pi^2\rho_i)^{\frac{1}{3}}$;, $\rho(\mathcal{R}) = \rho_p + \rho_n$ and $\mathcal{R} = \frac{\rho_p}{\rho_n}$. Then, here we can rewrite the two-body cluster term as,

$$\mathcal{E}_2 = \mathcal{E}_c^{NN} + \mathcal{E}_{\mathcal{T}}^{NN} + \mathcal{E}_{\mathcal{T}}^{N\Delta}, \tag{A3}$$

where (c and $\mathcal{T}$ stand for the central and tensor parts, respectively and $\alpha = LSJTM_T$)

$$\mathcal{E}_i^j = \frac{2}{\pi^4\rho(\mathcal{R})}\sum_\alpha |\langle m_{\tau_1}m_{\tau_2}|T, M_T\rangle|^2(2J+1) \times \frac{1}{2}\{1-(-1)^{L+S+T}\}\int_0^\infty r^2 dr \mathcal{V}_\alpha^{i,j}[r,\rho(\mathcal{R})]a_\alpha^{(1)^2}(r) \tag{A4}$$

and ($i = c, \mathcal{T}$ and $j = NN, N\Delta$)

$$\mathcal{V}_\alpha^{c,NN}[r,\rho(\mathcal{R})] = \frac{\hbar^2}{m}\left[f_\alpha^{(1)^2} + \frac{m}{\hbar^2}V_\alpha^c f_\alpha^{(1)^2}\right] \tag{A5}$$

$$\begin{aligned}\mathcal{V}_\alpha^{\mathcal{T},NN}[r,\rho(\mathcal{R})] = \Bigg\{&\frac{\hbar^2}{m}\Bigg[f_\alpha^{(2)^2} + \frac{m}{\hbar^2}\left(V_\alpha^c + 2V_\alpha^{\mathcal{T}} - V_\alpha^{LS}\right) \times f_\alpha^{(2)^2}\Bigg]a_\alpha^{(2)^2}(r) + \frac{\hbar^2}{m}\Bigg[f_\alpha^{(3)^2} + \frac{m}{\hbar^2} \\ &\times \left(V_\alpha^c - 4V_\alpha^{\mathcal{T}} - 2V_\alpha^{LS}\right)f_\alpha^{(3)^2}\Bigg]a_\alpha^{(3)^2}(r) + \Bigg[r^{-2}\Bigg(f_\alpha^{(2)^2} - f_\alpha^{(3)^2} + \frac{m}{\hbar^2}V_\alpha^{LS}f_\alpha^{(2)} \\ &\times f_\alpha^{(3)}\Bigg)\Bigg]b_\alpha^2\Bigg\}a_\alpha^{(1)^{-2}}(r)\end{aligned} \tag{A6}$$

$$\begin{aligned}\mathcal{V}_\alpha^{\mathcal{T},N\Delta}[r,\rho(\mathcal{R})] = &\left\{\frac{\hbar^2}{2\mu}\left[f_\alpha^{(1)^2} + \frac{\mu}{\mu_\Delta}\left(f_\alpha^{(4)^2} + \frac{6}{r^2}f_\alpha^{(4)^2}\right)\right]\right. \\ &\left. + (m_\Delta - m)c^2 f_\alpha^{(1)^2} + 2f_\alpha^{(1)}f_\alpha^{(4)}V_\alpha^{\mathcal{T},\Delta} + V_\alpha^c f_\alpha^{(1)^2}\right\}\end{aligned} \tag{A7}$$

$$a_\alpha^{(1)^2}[r,\rho(\mathcal{R})] = I_J^{M_T}[r,\rho(\mathcal{R})] \tag{A8}$$

$$a_\alpha^{(2)^2}[r,\rho(\mathcal{R})] = (2J+1)^{-1}\left\{(J+1)I_{J-1}^{M_T}[r,\rho(\mathcal{R})] + JI_{J+1}^{M_T}[r,\rho(\mathcal{R})]\right\} \tag{A9}$$

$$a_\alpha^{(3)^2}[r,\rho(\mathcal{R})] = (2J+1)^{-1}\left\{JI_{J-1}^{M_T}[r,\rho(\mathcal{R})] + (J+1)I_{J+1}^{M_T}[r,\rho(\mathcal{R})\right\} \tag{A10}$$

$$b_\alpha^2[r,\rho(\mathcal{R})] = 2J(J+1)(2J+1)^{-1}\left\{I_{J-1}^{M_T}[r,\rho(\mathcal{R})] - I_{J+1}^{M_T}[r,\rho(\mathcal{R})]\right\} \tag{A11}$$

$$I_J^{M_T}[r,\rho(\mathcal{R})] = \int d\mathbf{q}\mathcal{J}_J^2(rq)\mathcal{P}_{M_T}(q) \tag{A12}$$

$$\mathcal{P}_{M_T}(q) = \frac{2}{3}\pi\left[{k_F^i}^3 + {k_F^j}^3 - \frac{3}{2}\left({k_F^i}^2 + {k_F^j}^2\right)q - \frac{3}{15}\left({k_F^i}^2 - {k_F^j}^2\right)^2 q^{-1} + q^3\right] \tag{A13}$$

for $\frac{1}{2}|k_F^i - k_F^j| < q < |k_F^i + k_F^j|$ and

$$\mathcal{P}_{M_T}(q) = \frac{4}{3}\pi\min\left({k_F^i}^3, {k_F^j}^3\right) \tag{A14}$$

for $q < \frac{1}{2}|k_F^i - k_F^j|$ and

$$\mathcal{P}_{M_T}(q) = 0 \tag{A15}$$

for $q > \frac{1}{2}|k_F^i + k_F^j|$. The potential functions V_α^c, $V_\alpha^{\mathcal{T}}$, . . . and so on are given in Refs. [5,13]. Here our channel-dependent effective two-body interactions have different forms in terms of isospin projection $M_T(= -1, 1, 0)$ i.e., n-n, p-p, and n-p and the proton to neutron densities ratio $\mathcal{R}$.

As usual, we impose the normalization condition [2]:

$$\rho\int[G(r)-1]d\mathbf{r} = -1, \tag{A16}$$

where $G(r)$ is the two-body radial distribution function. This condition also plays the role of smallness parameter in the cluster expansion [2]. The channel break down of the above normalization constraint [13] has the following form:

$$\frac{1}{\pi^4\rho(\mathcal{R})}\sum_{\alpha,k}(2J+1)\frac{1}{2}[1-(-1)^{(L+S+T)}]|\langle m_{\tau_1}m_{\tau_2}|T,M_T\rangle|^2 \int_0^\infty r^2 dr\left[f_\alpha^{(k)^2}(r) - f_p^{M_T{}^2}(r)\right]a_\alpha^{(k)^2}(r) = -1. \tag{A17}$$

By minimizing the two-body energy $\mathcal{E}_2$ subject to the above constraint, we find the following sets of uncoupled,

$$g_\alpha^{(1)''} - \left[a_\alpha^{(1)''}/a_\alpha^{(1)} + m\hbar^{-2}\left(V_\alpha^c + \lambda\right)\right]g_\alpha^{(1)} = 0 \tag{A18}$$

and coupled,

$$\begin{aligned}g_\alpha^{(2)''} - \left[a_\alpha^{(2)''}/a_\alpha^{(2)} + m\hbar^{-2}\left(V_\alpha^c + 2V_\alpha^{\mathcal{T}} - V_\alpha^{LS} + \lambda\right)\right. \\ \left. + r^{-2}b_\alpha^2/a_\alpha^{(2)^2}\right]g_\alpha^{(2)} + \left(r^{-2} - \tfrac{1}{2}m\hbar^{-2}V_\alpha^{LS}\right) \\ \times b_\alpha^2\left\{a_\alpha^{(2)}a_\alpha^{(3)}\right\}^{-1}g_\alpha^{(3)} = 0\end{aligned} \tag{A19}$$

$$\begin{aligned}g_\alpha^{(3)''} - \left[a_\alpha^{(3)''}/a_\alpha^{(3)} + m\hbar^{-2}\left(V_\alpha^c - 4V_\alpha^{\mathcal{T}} - 2V_\alpha^{LS} + \lambda\right)\right. \\ \left. + r^{-2}b_\alpha^2/a_\alpha^{(3)^2}\right]g_\alpha^{(3)} + \left(r^{-2} - \tfrac{1}{2}m\hbar^{-2}V_\alpha^{LS}\right) \\ \times b_\alpha^2\left\{a_\alpha^{(2)}a_\alpha^{(3)}\right\}^{-1}g_\alpha^{(2)} = 0\end{aligned} \tag{A20}$$

Euler-Lagrange differential equations, where

$$g_\alpha^{(k)} = a_\alpha^{(k)}f_\alpha^{(k)}. \tag{A21}$$

The E-L differential equations for N-Δ channels are given in Ref. [1]. The Lagrange multiplier λ has been introduced to satisfy the normalization condition. The constraint is incorporated by solving the above E-L equations only out to certain distances, until the logarithmic derivative of correlation functions matches those of $f_p^{M_T}(r)$ and then we set the correlation functions equal to $f_p^{M_T}(r)$. So there is no free parameter in our LOCV formalism, i.e., the healing distances are determined directly by the constraint and the initial conditions.

[1] M. Modarres and N. Rasekhinejad, Phys. Rev. C **72**, 014301 (2005).
[2] B. D. Day, Rev. Mod. Phys. **50**, 495 (1978); J. W. Clark, Prog. Part. Nucl. Phys. **2**, 89 (1979); V. R. Pandharipande and R. B. Wiringa, Rev. Mod. Phys. **51**, 821 (1979).
[3] C. R. Chen, G. L. Payne, J. L. Friar, and B. F. Gibson, Phys. Rev. C **33**, 1740 (1986); A. Stadler, W. Glöckle, and P. U. Sauer, *ibid*. **44**, 2319 (1991).
[4] J. Carlson, Phys. Rev. C **38**, 1879 (1988); S. C. Pieper, R. B. Wiringa, and V. R. Pandharipande, *ibid*. **46**, 1741 (1992); B. S. Pudliner, V. R. Pandharipande, J. Carlson, S. C. Pieper, and R. B. Wiringa, *ibid*. **56**, 1720 (1997); A. Kievsky, M. Viviani, and S. Rosati, Nucl. Phys. **A551**, 241 (1993); S. C. Pieper, R. B. Wiringa, and J. Carlson, Phys. Rev. C **70**, 054325 (2004); S. C. Pieper, Phys. Rev. Lett. **90**, 252501 (2003); S. C. Pieper, K. Varga, and R. B. Wiringa, Phys. Rev. C **66**, 044310 (2002); S. C. Pieper and R. B. Wiringa, Annu. Rev. Nucl. Part. Sci. **51**, 53 (2001).
[5] J. C. Owen, R. F. Bishop, and J. M. Irvine, Ann. Phys. (NY) **102**, 170 (1976); M. Modarres and J. M. Irvine, J. Phys. G **5**, 511 (1979); M. Modarres and G.H. Bordbar, Phys. Rev. C **58**, 2781 (1998); M. Modarres and J. M. Irvine, J. Phys. G **5**, L7 (1979).
[6] R. V. Reid, Ann. Phys. **50**, 411 (1969); B. D. Day, Phys. Rev. C **24**, 1203 (1981); A. M. Green, J. A. Niskanan and M. E. Sainio, J. Phys. G **4**, 1055 (1978).
[7] B. Friedman and V. R. Pandharipande, Nucl. Phys. **A361**, 502 (1981); R. B. Wiringa, V. Ficks, and A. Fabrocini, Phys. Rev. C **38**, 1010 (1988).
[8] I. E. Lagaris and V. R. Pandharipande, Nucl. Phys. **A359**, 331 (1981).
[9] R. B. Wiringa, R. A. Smith, and T. L. Ainsworth, Phys. Rev. C **29**, 1207 (1984).
[10] R. B. Wiringa, V. G. J. Stoks, and R. Schiavilla, Phys. Rev. C **51**, 38 (1995).
[11] V. Stoks and J. J. de Swart, Phys. Rev. C **52**, 1698 (1995).
[12] K. E. Schmidt and V. R. Panharipande, Phys. Lett. **B87**, 11 (1979); A. Akmal, V. R. Pandharipande, and D. G. Ravenhall, Phys. Rev. C **58**, 1804 (1998).
[13] M. Modarres, J. Phys. G **19**, 1349 (1993); M. Modarres and H. R Moshfegh, Phys. Rev. C **62**, 044308 (2000); G. H. Bordbar and M. Modarres, J. Phys. G: Nucl. Part. Phys. **23**, 1631 (1997); Phys. Rev. C **57**, 714 (1998); H. R. Moshfegh and M. Modarres, J. Phys. G **24**, 821 (1998).
[14] R. F. Bishop, C. Howes, J. M. Irvine, and M. Modarres, J. Phys. G **4**, 1709 (1978).
[15] M. Modarres, J. Phys. G **10**, 251 (1984).
[16] J. W. Negele, Phys. Rev. C **1**, 1260 (1970).
[17] H. Kümmel, K. H. Lührmann, and J. G. Zabolitzky, Phys. Rep. **36**, 1 (1978).
[18] A. Fabrocini, F. Arias de Saavedra, G. Có, and P. Folgarait, Phys. Rev. C **57**, 1668 (1998).
[19] A. Fabrocini, F. Arias de Saavedra, and G. Có, Phys. Rev. C **61**, 044302 (2000).
[20] G. Có, A. Fabrocini, S. Fantoni, and E. Lagaris, Nucl. Phys. **A549**, 439 (1992).
[21] G. Có, A. Fabrocini, and S. Fantoni, Nucl. Phys. **A568**, 73 (1992).
[22] F. Arias de Saavedra, G. Có, A. Fabrocini, and S. Fantoni, Nucl. Phys. **A605**, 359 (1996).
[23] F. Arias de Saavedra, G. Có, and A. Fabrocini, Phys. Rev. C **63**, 064308 (2001).
[24] F. Arias de Saavedra, G. Có, and M. M. Renis, Phys. Rev. C **55**, 673 (1997).
[25] L. Coraggio, N. Itaco, A. Covello, A. Gargano, and T. T. S. Kuo, Phys. Rev. C **68**, 034320 (2003).
[26] L. Coraggio, A. Covello, A. Gargano, N. Itaco, T. T. S. Kuo, and R. Machleidt, Phys. Rev. C **71**, 014307 (2005).
[27] R. Roth, T. Neff, H. Hergert, and H. Feldmeier, Nucl. Phys. **A745**, 3 (2004).
[28] H. de Vries, C. W. de Jager, C. de Vries, At. Data Nucl. Data Tables **36**, 495 (1987).
[29] M. Modarres and H. R. Moshfegh, Prog. Theor. Phys. **112**, 21 (2004); H. R. Moshfegh and M. Modarres, Nucl. Phys. **A759**, 79 (2005).
[30] V. Stoks and J. J. de Swart, Phys. Rev. C **47**, 761 (1993); **52**, 1698 (1995); V. G. J. Stoks, R. A. M. Klomp, C. P. F. Terheggen, and J. J. de Swart, *ibid*. **49**, 2950 (1994); V. G. J. Stoks, R. A. M. Klomp, M. C. M. Rentmeester, and J. J. de Swart, *ibid*. **48**, 792 (1993).
[31] T. Brody and M. Moshinsky, *Tables of Transformation Brackets* (Mexico Instituto de Fisica, Mexico City, 1960).
[32] E. Feenberg, *Theory of Quantum Fluids* (Academic Press, New York, 1969); M. A. Preston and R. K. Bhaduri, *Structure of the Nucleus* (Addison-Wesley, Reading, MA, 1975).